

Case Study

CFD Analysis of a Classical Venturi Model with Ansys Discovery Software

Maggie Crawford, Sunil Rathagirishnan, Adni Zhao, Sonia Marin, and Andrew Gryguc

University of Waterloo

Edited by the Ansys Academic Development Team

education@ansys.com

Ansys Software Used

This resource uses Ansys Discovery™, a 3D product simulation software.

Summary

This case study involves internal fluid flow in a converging-diverging nozzle with varying parameters using the Ansys Discovery software. The goal is to understand how pressure and velocity are affected by the parameters of the nozzle and in the different locations along the venturi tube. The venturi tube covers fundamental concepts using Bernoulli’s principles to concepts used in de Laval nozzles.

It was discovered that as diameter of the tube constricts, the velocity of fluid flow increases while pressure decreases. Thus, the two factors are inversely related, as stated by Bernoulli’s principle. Additionally, the turbulence in the model varies depending on which side of the tube is connected to the vacuum. When the gradually sloped end is connected, less turbulence is present because the geometry does not change as abruptly as with the steeper slope. This allows the air to move in a smoother manner. Comparison to experimental data is included in this document.

Table of Contents

1. Introduction.....	3
1.1 Fluid Dynamics.....	3
1.2 Venturi Tube.....	3
2. Concepts.....	3
2.1 Bernoulli’s Principle	3
2.2 Conservation of mass.....	4
2.3 Venturi tube calculations	4
3. Venturi Design ISO standards	5
4. Case Study Venturi Geometry	6
4.1 Changes in Throat and Opening Diameters	7
5. Experiment Setup.....	8
5.1 Materials.....	8
5.2 Procedures.....	9
5.3 Results.....	9
5.3.1 Air Velocity Profile	9
5.3.2 Pressure	10
6. Simulation Setup in Ansys Discovery Software.....	10
6.1 Pre-Processing	10
6.2 Running simulation and visualizing results	11
7. Simulation Results	12
7.1 Velocity Profile	12
7.2 Pressure	16
7.3 Turbulence model sensitivity study	17
7.3.1 Straight Venturi Tube Analysis.....	18
7.3.2 Twisted Venturi Tube Analysis.....	19
8. Analysis.....	21
8.1 Air Velocity Profile.....	21
8.2 Sources of Error	22
8.2.1 Air leak	22
8.2.2 Meshing.....	23
8.2.3 Refine Mode	23
8.2.4 3D Printing Shrinking/Surface Roughness.....	24
8.2.5 Turbulence.....	24
9. Conclusions	24
10. References.....	25

1. Introduction

1.1 Fluid Dynamics

Fluid dynamics is an important field of study in engineering. Matter exists in three phases, and fluid dynamics considers the motion of both gases and liquids. These concepts are seen in many applications; consider a Formula 1 car's aerodynamics (Figure 1a) or a blood vessel in the human body (Figure 1b). Understanding how fluids behave helps us predict, control, and optimize countless systems in engineering, nature, and daily life.

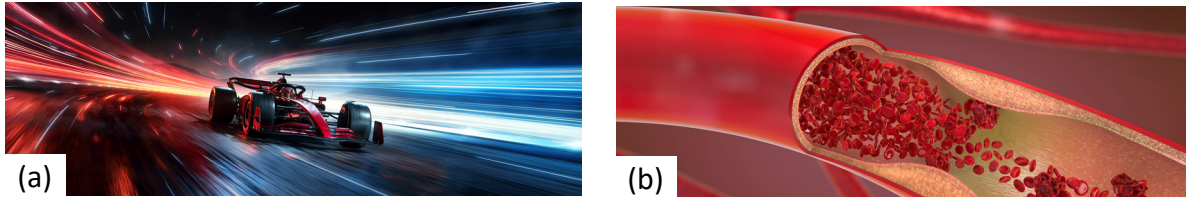


Figure 1: Examples of Fluid Dynamics Applications
(a) F1 car (b) blood vessels moving in arteries

1.2 Venturi Tube

A venturi tube is a measuring instrument used to determine the flow rate in fluids accurately (see details in Figure 4). The tube consists of a converging section, throat and diverging section. By using Bernoulli's equation, the measurements of pressure can be used to determine the flow rate in the different sections of the tube.

2. Concepts

2.1 Bernoulli's Principle

The Bernoulli equation is derived from the principle of conservation of energy for flowing fluids. It describes a relation between fluid speed, pressure and potential energy. The equation balances the different forms of energy; kinetic, potential and internal energies, through varying cross-sections and heights. Bernoulli's equation is defined for an incompressible frictionless fluid and hence does not apply for boundary layer calculations .

The principle states that for an incompressible and frictionless fluid, the kinetic energy ($\frac{1}{2}\rho V^2$), potential energy (ρgh), and pressure (p) remain constant along a streamline, shown in Equation 1.

$$p_0 = p + \frac{1}{2}\rho V^2 + \rho gh \quad \text{Eq. 1}$$

Where:

- p_0 is the stagnation pressure which is constant at any point where velocity is 0. It is the sum of the static pressure p and dynamic pressure q .
- ρ is the fluid density.
- V is the fluid velocity.
- V_0 is the velocity at the stagnation point
- g is the acceleration due to gravity.
- h is the height above a reference point.

It must be noted that Equation 1 represents the simplified form in which the term ρgz with elevation z considered zero, cancels out.

As the tube constricts, the water will move faster and be under less pressure. A simple explanation can be given by high pressure pushing the faster moving fluid. Assuming there is no change in the height of the fluid, the potential energy terms can cancel out.

Additionally, by rearranging Bernoulli's principle, we can see that while all other parameters remain constant, as velocity is increased, the pressure in that location will decrease.

As V increases, p becomes more negative (decreases).

$$p_0 = p + \frac{1}{2}\rho V^2 + \rho gh$$

$$-p = -p_0 + \frac{1}{2}\rho V^2 + \rho gh$$

2.2 Conservation of mass

Relating to conservation of mass and Bernoulli's, the continuity equation states that the mass flow of a fluid must remain constant from one cross-section to another in a tube, for an incompressible fluid (Equation 2).

$$A_1 V_1 = A_2 V_2 \quad \text{Eq. 2}$$

Where:

- A is the cross-sectional area
- V is the velocity of the fluid

This also explains how the velocity of the fluid increases as the cross-sectional area decreases to keep the equation balanced, such as in Figure 2.

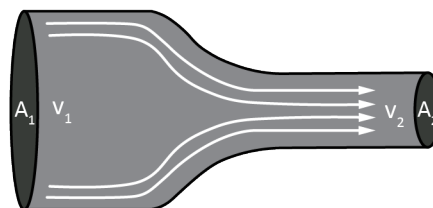


Figure 2: Schematic of Converging Nozzle

2.3 Venturi tube calculations

The analytical calculation of the outlet velocity in a venturi tube is outlined below.

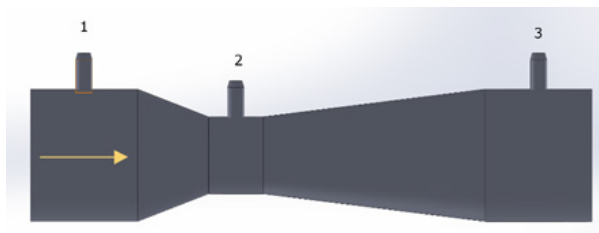


Figure 3: Venturi Example Model

Assuming Bernoulli's equation holds along the center streamline (shown as the dashed line in Figure 4):

$$p_1 + \frac{1}{2}\rho V_1^2 + \rho gh_1 = p_2 + \frac{1}{2}\rho V_2^2 + \rho gh_2$$

Since the heights of both points are assumed to be the same, there is no gravitational effect and as such, Bernoulli's equation reduces to:

$$p_1 + \frac{1}{2}\rho V_1^2 = p_2 + \frac{1}{2}\rho V_2^2$$

Using the conservation of mass equation for an incompressible fluid:

$$A_1 V_1 = A_2 V_2 \text{ and } A = \frac{\pi}{4}d^2 \text{ thus } V_1 = \beta^2 V_2$$

Where $\beta = d_2/d_1$ is the diameter ratio

By substitution, we get the Outlet Velocity Equation for the Venturi tube:

$$V_2 = \left[\frac{2\Delta p}{\rho(1 - \beta^4)} \right]^{\frac{1}{2}} \quad \text{Eq. 3}$$

3. Venturi Design ISO standards

The International Organization for Standardization (ISO) provides standardized regulations agreed upon by experts. ISO 5167 provides a baseline for the standard venturi tube [1].

The venturi tube consists of the sections shown below in Figure 4.

- Entrance Cylinder (A): A cylindrical section where the fluid first enters.
- Converging Section (B): A conical section where the fluid velocity increases and pressure decreases. This section has an included angle of $21^\circ \pm 1^\circ$.
- Cylindrical Throat (C): The narrowest section where the fluid velocity is at its maximum and pressure is at its minimum. The length of this section is equal to the throat diameter (d) $\pm 0.03d$.
- Diverging Section (D): A conical section where the fluid velocity decreases and pressure increases. This section typically has an included angle between 7° and 15° , with an angle between 7° and 8° being recommended.

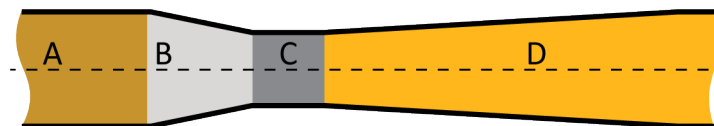


Figure 4: ISO Standard Design (adapted from Reference [1])

Table 1: Sample Venturi Dimensions

Design	Diameters (mm)			Angle		Lengths (mm)			Inlet Velocity (m/s)	Fluid
	Inlet	Throat	Ratio	Converging	Diverging	Throat	Converging	Diverging		
1	30.5	15.25	0.5	21	7	15.25	41.175	61	30	Air
2	30.5	6.1	0.2	20	8	6.1	66.06	101.5	30	Air
3	30.5	20.33	0.67	15	6	20.33	27.89	91.5	30	Air

4. Case Study Venturi Geometry

Two variations of the Venturi tube were used for this experiment. Venturi 1 is straight and resembles the standard Venturi, while Venturi 2 is bent at the throat (Figure 5). Both variations have the same inlet and outlet dimensions as well as α and β angles. These two tubes give us four different configurations, since the inlet and outlet definitions can be switched to create a new setup. The dimensions of each Venturi are tabulated below.

Table 2: Venturi Dimensions

Venturi	Diameters (mm)			Angle		Lengths (mm)			Inlet Velocity (m/s)	Fluid
	Inlet	Throat	Ratio	Converging	Diverging	Throat	Converging	Diverging		
1	31.0	10.0	0.32	27.7	9.93	39.00	20.00	60.00	21	Air
2	31.0	10.0	0.32	9.93	27.7	39.00	60.00	20.00	21	Air

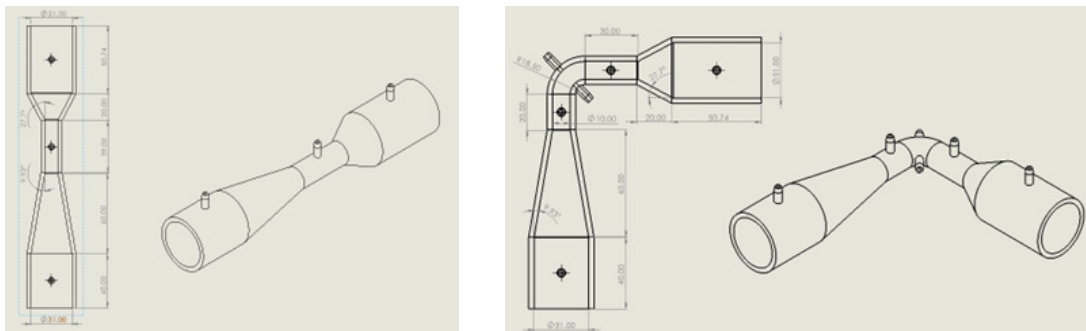
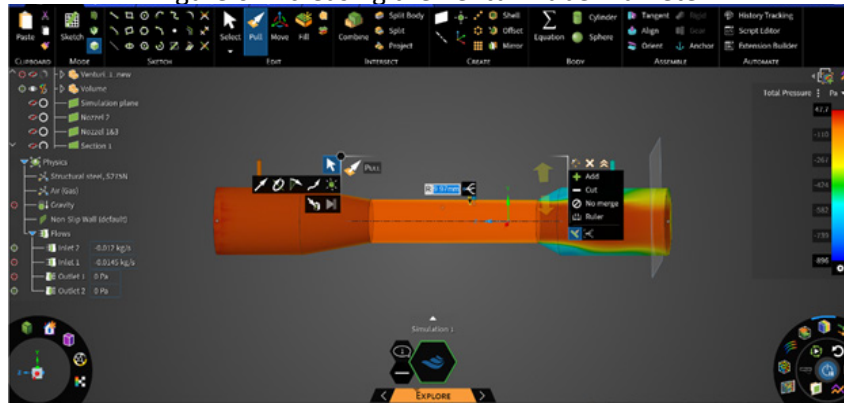


Figure 5: Venturi Design 1 (Straight Tube-left) and Design 2 (Bent Tube-right)

4.1 Changes in Throat and Opening Diameters

Using the design exploration capabilities within the Ansys Discovery software, the pull tool changes the diameter of *e.g.* the central tube of the Venturi (Figure 6) to explore how the geometry affects the results of the simulation.

Figure 6: Increasing the Venturi Tube Diameter



Widening the throat diameter while keeping the inlet and outlet diameters constant results in a max pressure increase and max velocity decrease. This is intuitive given that pressure and velocity are inversely proportional according to Bernoulli's principle. Conversely, constricting the throat diameter while keeping the inlet and outlet diameters constant results in a max pressure decrease and max velocity increase. The same results would occur if the throat remained unchanged while the inlet and outlet diameters were modified; this is true for both Venturis 1 and 2.

Changing the diameters also implies a change in the converging and diverging angles within the tube. This would affect the flow pattern and turbulence levels in each configuration. For both the straight and bent tubes, turbulence is highest when the outlet angle is steeper than the inlet angle. The sudden change in flow geometry leaves more backflow, thus resulting in higher turbulence and flow separation. Increasing the throat diameter reduces this effect while decreasing it would strengthen the effect.

An interesting theoretical edge case could be creating a Venturi tube that reaches Mach speed. To reach Mach 1, the throat of the tube would have to be sufficiently choked in order to create a pressure ratio that is capable of reaching such a high velocity. For instance, having the air flow from a high-pressure reservoir into a vacuum chamber could choke the throat.

To track the flow rate, pressure modulation can be used. The pressure naturally changes as it goes through the tube and can be calculated using a substitution of Bernoulli's equation into the continuity equation for Volumetric Flow Rate (Eq. 4).

$$Q = A_2 \sqrt{\frac{2(P_1 - P_2)}{\rho}} \quad \text{Eq. 4}$$

Where:

- Q is volumetric flow rate
- A_2 is cross-sectional area at the throat
- P_1 is pressure at the inlet
- P_2 is pressure at the throat
- ρ is fluid density

5. Experiment Setup

5.1 Materials

The test setup for the Venturi tube experiment consists of a controlled airflow system and measurement instruments to analyze pressure and velocity changes. The vacuum source generates airflow through the 3D-printed PLA Venturi tube, creating a pressure differential as the air accelerates through the constricted section. A manometer is connected to pressure ports at different points along the Venturi tube to measure the pressure drop between the inlet, throat, and outlet. An anemometer is positioned at the exit of the Venturi tube to measure airflow velocity.

Referring to Figure 7a, pressure tap 1 and 3 allow for pressure measurements at the diverging and converging ends, respectively, while pressure tap 2 takes measurements at the throat.

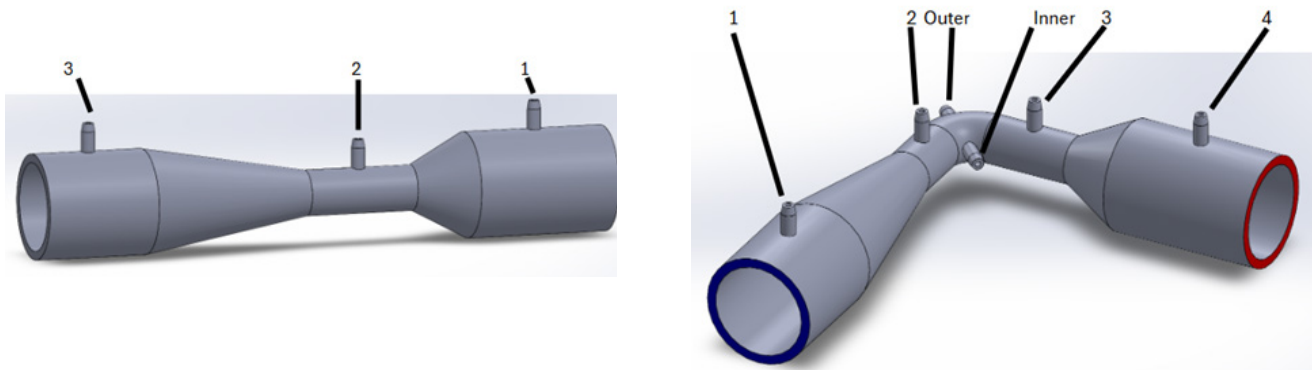


Figure 7: Pressure Tap Placement for (a) Venturi 1 and (b) Venturi 2

In Figure 7b, pressure taps 1 and 4 allow for pressure measurement at the converging and diverging ends. Pressure taps 2 and 3 take measurements at the throat before turning and after turning, respectively. The outer and inner pressure taps take measurements of the pressure gradient across the tube section at the turning point.

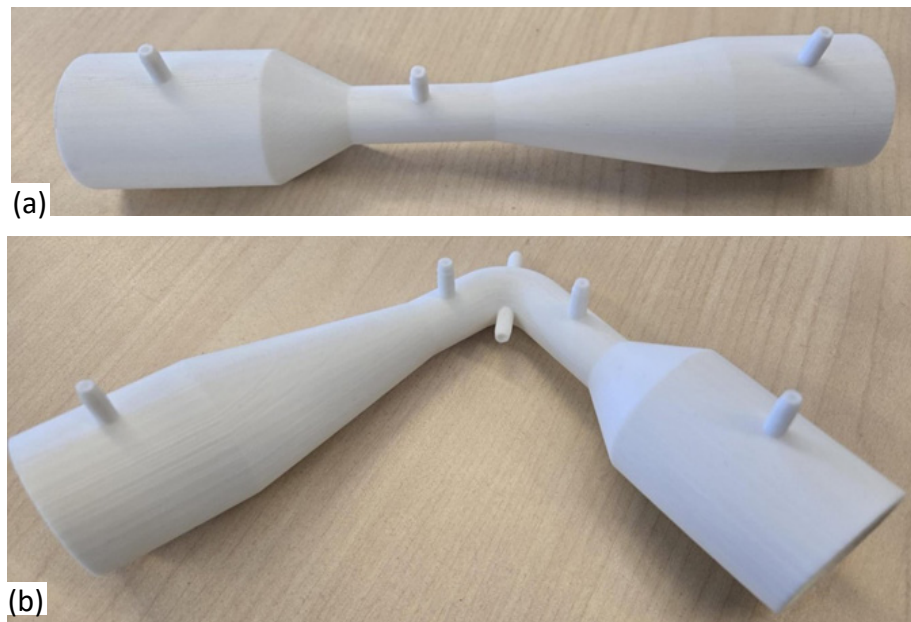


Figure 8: 3D Print of (a) Venturi tube 1 and (b) Venturi tube 2

5.2 Procedures

The experimental setup was designed to analyze the air velocity profile and pressure distribution within a 3D-printed Venturi tube (Figures 8a and b) under controlled airflow conditions. The Venturi tube was securely connected to a vacuum source to minimize leakage. For velocity measurements, an anemometer was positioned at the inlet, with its sensing element placed at the edge. Airspeed readings were recorded along the outlet edge at varying distances from the center, allowing for the determination of an average velocity profile. This process was repeated at multiple positions, and the velocity data was plotted against radial distance to visualize airflow characteristics.

For pressure measurements, a manometer was calibrated in kilopascals (kPa) prior to data collection. The vacuum was activated, and the manometer tube was connected sequentially to each pressure port along the Venturi tube. Pressure readings were recorded once stabilization was achieved. Two configurations were tested: Config. 1, where the steeper slope side was connected to the vacuum, and Config. 2, where the longer sloped side was connected. The collected pressure data provided insights into the pressure variations along the Venturi tube, validating theoretical expectations based on Bernoulli's principle.

5.3 Results

5.3.1 Air Velocity Profile

As shown in Figures 9a and b, Series 1 is the air velocity with turbulence while Series 2 is the uniform approximation of the air velocity at the outlets. Series 1 exhibits a nonlinear profile across the cross section; the turbulent velocity decreases as it approaches the internal boundary of the Venturi tube, which implies that the friction or viscous drag has restricted fluid flow in contact with the solid boundaries.

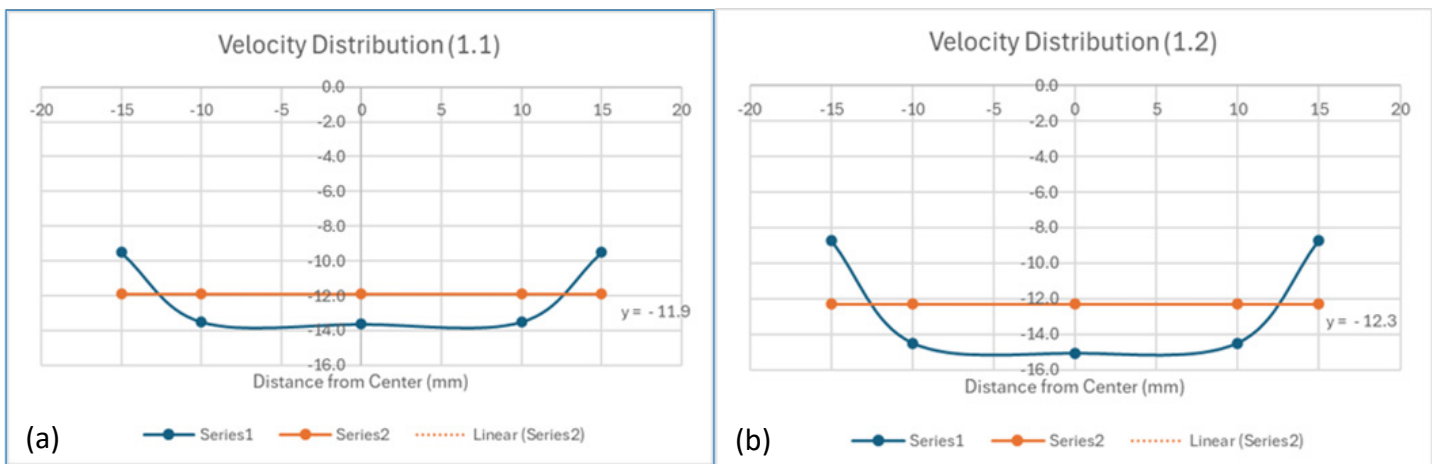


Figure 9: Inlet Velocity Profile for Venturi 1
(a) Config. 1 (b) Config. 2

For all collections, the same vacuum was used which produced an outlet suction airspeed of approximately 12 m/s, found experimentally, as the airflow profile.

5.3.2 Pressure

Table 3 displays the measured pressure values of the two Venturi tube geometries at corresponding pressure taps, where configuration 1 connected the vacuum with the steep ended slope and configuration 2 connected the vacuum with the gradually ending slope. It can be observed that the end connected to the vacuum maintains a consistent pressure of around 10kPa while the other end maintains a pressure of near 0 kPa. In other words, the vacuum has a constant suction power and the end exposed to the environment has close to ambient pressure.

Table 3: Experimental Pressure Data

Venturi	Config.	Pressure Tap #	Experimental Pressure (kPa)
1	1	1	-10.68
		2	-11.00
		3	-0.10
	2	1	-0.10
		2	-13.60
		3	-10.00
2	1	1	-0.03
		2	-6.20
		3	-11.70
		4	-11.10
		Inner	-16.50
		Outer	-4.40
	2	1	-10.50
		2	-13.90
		3	-6.80
		4	-0.04
		Inner	-20.60
		Outer	-5.80

6. Simulation Setup in Ansys Discovery Software

6.1 Pre-Processing

Firstly, the CAD geometry (*.STEP) of the internal fluid domain is imported into the Ansys Discovery software. Please note that if you had the venturi geometry itself, extracting the fluid volume would initially be required. For more information, please see this tutorial: [Fluid Flow Simulation Using Ansys Discovery | Ansys Courses](#).

Subsequently, the flow simulation is selected from the Simulation tab, defining a mass flow rate of a negative value (since the flow is a suction air flow) as flow inlet and a 0 Pa (relative pressure) flow outlet at the opposite opening, as shown in Figure 10. Next, the default medium water was changed to air.

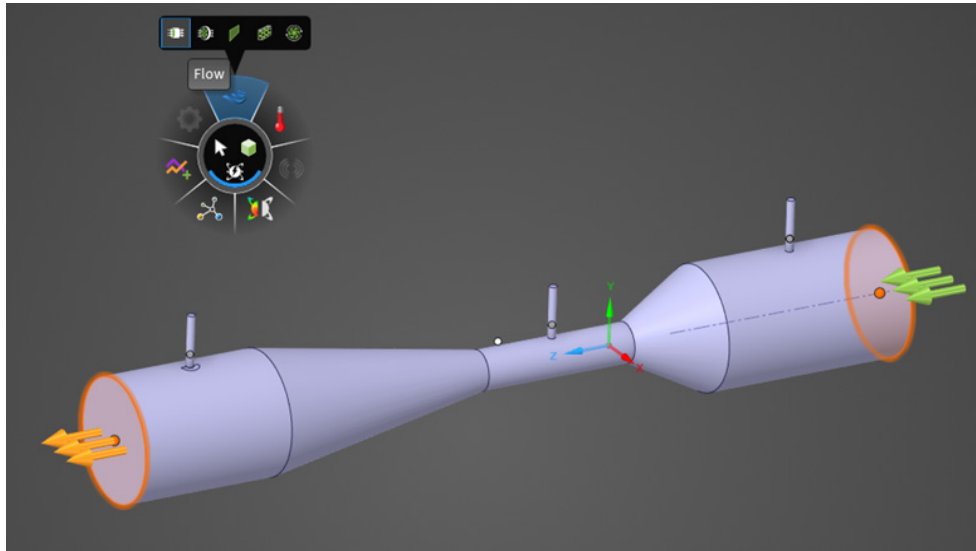


Figure 10: Inlet and Outlet Flow Conditions Applied

6.2 Running simulation and visualizing results

After solving the flow problem, simulation results were analyzed using various visualization tools. Different data representations, including contour plots, streamlines, particle tracking, direction fields, and vector fields, were accessed by selecting or deselecting the corresponding icons on the outer ring of the “Run Simulation” button. A plane section view was generated to visualize internal venturi flow parallel to the airflow. The simulation results were adjusted by selecting either pressure or velocity from the drop-down menu located at the top of the color scale on the right side of the screen. Specific values of pressure or velocity at any given point were obtained by hovering over the desired location, with the corresponding value displayed on the color scale (see Figure 11).

To simulate an alternative configuration, the inlet and outlet conditions were modified by selecting the green “Exclude from simulation” circle next to the boundary conditions and re-defining the parameters with the inlet and large outlet swapped. To facilitate identification, the configurations were labeled as inlet 1, outlet 1 or inlet 2, outlet 2.

To more accurately represent the boundary conditions of the physical experiment, the weighted mass flow rate of each Venturi tube design has been derived from the measured average inlet air velocity relative to the cross-section area and density of the air. It is identified that the standard Venturi tube has a calculated inlet mass flow rate of 0.012 kg/s and the twisted Venturi tube has a rate of 0.01 kg/s instead.

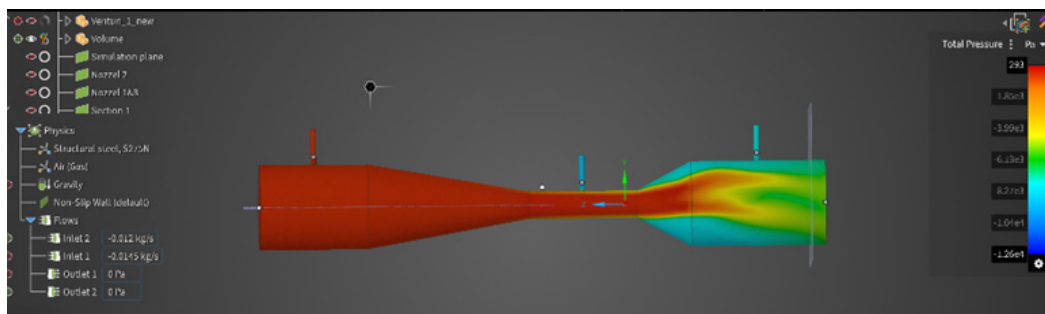


Figure 11: Total Pressure Results in Cross-Sectional View

7. Simulation Results

7.1 Velocity Profile

In Table 4, Config. 1 is where the steeper slope side was connected to the vacuum, and Config. 2 is where the longer sloped side was connected.

The table shows that the error rate between the experimental results and the simulation results is higher for the twisted Venturi tube design (Venturi 2) than the standard Venturi tube (Venturi 1). This phenomenon is expected as the twisted Venturi tube may involve more complex turbulent behavior that cannot be accurately captured by the simulation.

It is also worth pointing out from Figures 12 and 13 that the simulated velocity profile tends to deviate more from the physical measurements as it moves away from the center of the cross section, except for the second configuration of the twisted Venturi tube. It implies that the simulation may become less accurate when simulating fluid dynamics near the boundary.

Table 4: Velocity Profile Data (Raw)

Venturi	Config.	Distance from center (mm)	Experimental Pressure (m/s)	Simulation (m/s)	% Absolute Difference
1	1	0	-13.6	-13.9	2%
		10	-13.5	-13.8	2%
		15	-9.5	-12.6	28%
	2	0	-15.1	-15.2	1%
		10	-14.5	-15.2	5%
		15	-8.7	-13.3	42%
2	1	0	-11.65	-11.5	1%
		10	-9.95	-11.5	14%
		15	-10.5	-11.3	7%
	2	0	-11.5	-11.6	1%
		10	-10.6	-11.6	9%
		15	-10.4	-10.6	2%

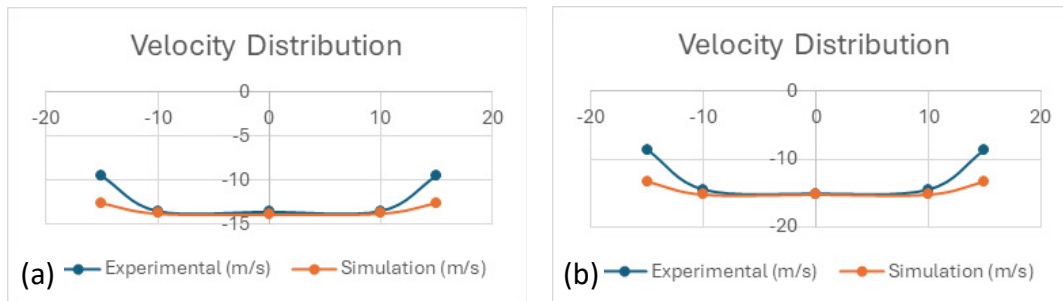


Figure 12: Venturi 1 Velocity Profiles
 (a) Config. 1 and (b) Config. 2

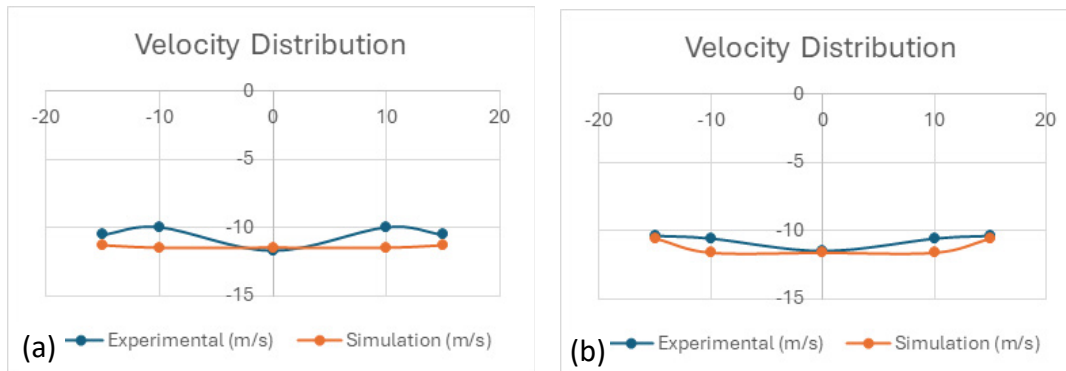


Figure 13: Venturi 2 Velocity Profiles
 (a) Config. 1 and (b) Config. 2

Each distance represents an offset ring from the center face of the Venturi inlet (schematic in Figure 13 and simulation result example in Figure 14). For instance, 10mm distance implies a circle with a radius of 10mm with its origin at the inlet face's center. A distance of 0mm implies the center origin itself.

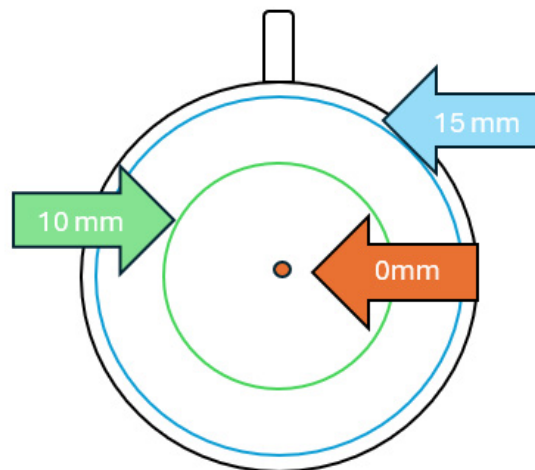


Figure 13: Inlet Cross Section

Most simulation values follow a similar trend as the experimental values. Given that the velocity varies depending on which direction from the origin the distance is measured from, an average velocity across the entire ring was taken.

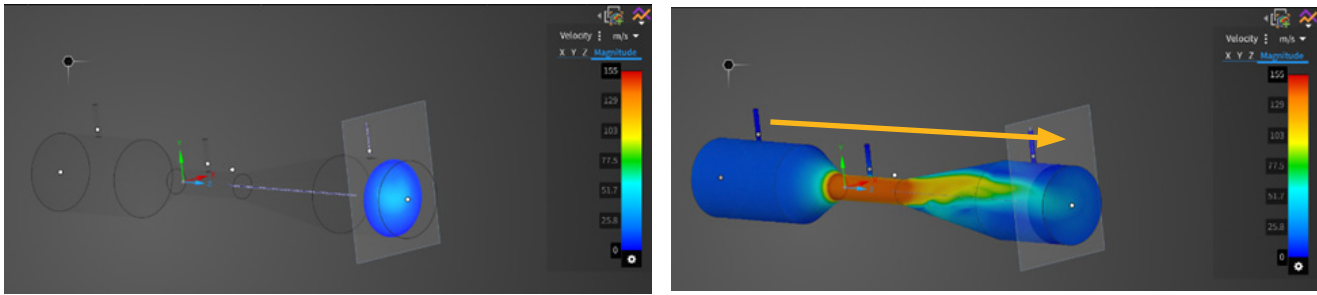


Figure 14: Inlet Velocity Profile of Venturi 1. Flow direction indicated by yellow arrow

By comparing Figures 15a and b, it can be found that the standard Venturi tube exhibits an overall axially symmetrical velocity profile near the physical outlet. However, the twisted venturi tube model (Figures 16a and b) did not exhibit such characteristic, since the presence of the corner interrupted symmetry between the left boundary layer and the right boundary layer.

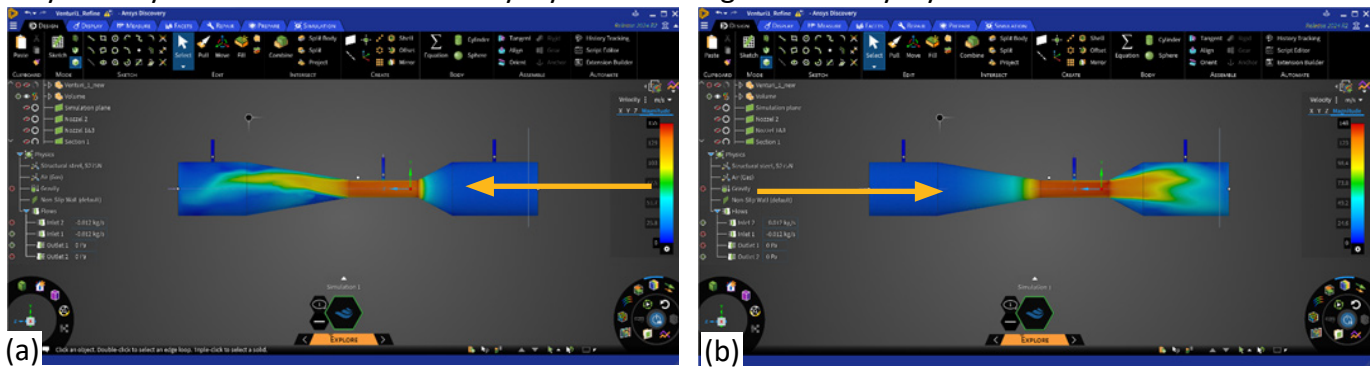


Figure 15: Venturi tube 1 Velocity Gradient Results. Flow direction indicated by yellow arrows
 (a) Config. 1 and (b) Config. 2

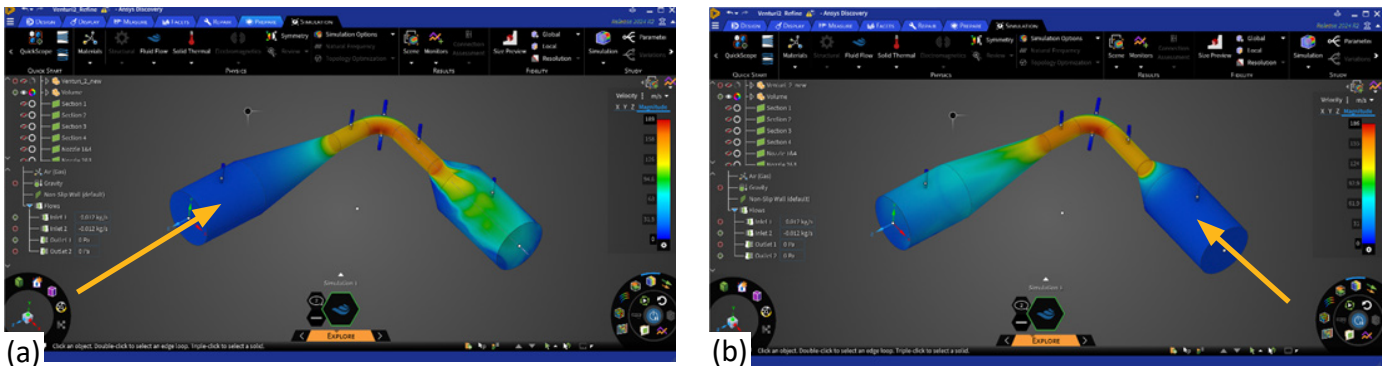


Figure 16: Venturi tube 2 Velocity Gradient Results. Flow direction indicated by yellow arrows
 (a) Config. 1 and (b) Config. 2

A more accurate comparison to the experiment readings would have been to take simulation monitors across distinct points on the offset rings. Since it is not feasible to take every possible point along the offset circles in practice, only 4 points were recorded on the edges of each ring during the experiment. Figure 17 symbolizes where these data points were measured in the simulation.

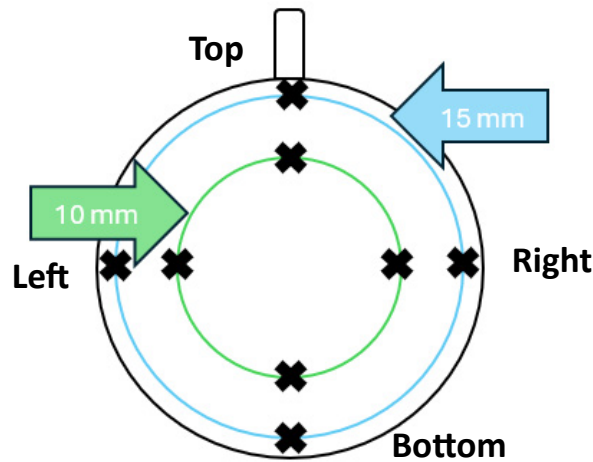


Figure 17: Venturi 2 Outlet Velocity Profile Investigation

Arrows indicate distance from center of tube. Direction labels are added for clarity for Table 5 data

As seen from Table 5, there exists relatively large absolute difference between experimental data and simulation data¹, which is potentially caused by limited precision in manual experimental data collection. Nonetheless, the experimental data and the simulation data show relatively similar trends along the horizontal direction or along the vertical direction with the experimental data point. The left 10 mm position been identified as an outlier. In general, the simulation and the experiment results have similar trends, which implies that the velocity profile of the twisted Venturi tube is asymmetrically distributed.

Table 5: Cross-section Velocity Data Comparison from Venture tube 2 Config. 2

Location (Position, Distance)	Experiment (m/s)	Simulation (m/s)	% Absolute Difference
Center, 0mm	-13.6	-13.9	2
Top, 10mm	10.6	13.8	30.19
Top, 15 mm	10.8	14.0	29.63
Bottom, 10 mm	10.2	13.7	34.31
Bottom, 15 mm	9.3	12.5	34.41
Left, 10 mm	9.7	13.8	42.27
Left, 15 mm	10.1	12.5	23.76
Right, 10 mm	11.6	13.8	18.97
Right, 15 mm	12.6	14	11.11

¹ Only values from Venturi tube 2, configuration 2 were taken due to time constraints

7.2 Pressure

Pressure readings were taken as an average across the face of each pressure tap and closer to the base (Figures 18 and 19). The data and comparison can be found in Table 6. It was discovered that the pressure increased with each subsequent pressure tap in configuration 1 and decreased in configuration 2. This follows intuition since readings taken closest to the vacuum should experience lower pressure than readings taken further from it. Although pressure tap 1 of Venturi 2 configuration 1 and pressure tap 4 of Venturi 2 configuration 2 show the highest percentage of absolute difference, both were located near the physical inlet of their configuration and had near ambient pressure. The deviation of the experimental data from the experimental result may be a result of how the Ansys Discovery software approximates near ambient fluid dynamics.

Table 6: Comparison of Internal Pressure Data

Venturi	Config.	Pressure Tap #	Experimental Pressure (kPa)	Simulation Pressure (kPa)	% Absolute Difference
1	1	1	-10.68	-0.11	10%
		2	-11.00	-10.20	8%
		3	-0.10	-7.7	32%
	2	1	-0.10	-8.18	20%
		2	-13.60	-10.60	25%
		3	-10.00	-0.11	10%
2	1	1	-0.03	-0.07	80%
		2	-6.20	-6.90	11%
		3	-11.70	-8.30	34%
		4	-11.10	-6.00	55%
		Inner	-16.50	-17.50	6%
		Outer	-4.40	-3.00	38%
	2	1	-10.50	-7.00	40%
		2	-13.90	-8.70	46%
		3	-6.80	-4.00	52%
		4	-0.04	-0.07	60%
		Inner	-20.6	-17.70	15%
		Outer	-5.8	-4.29	30%

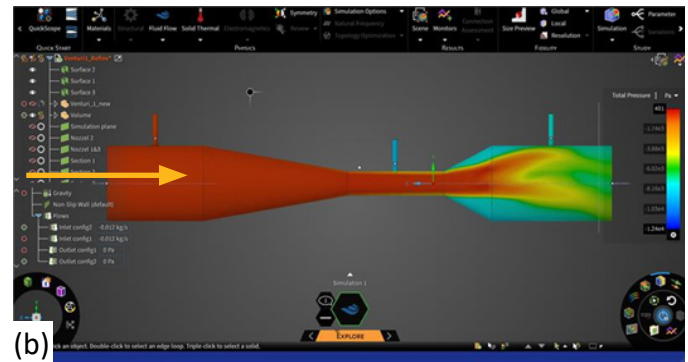
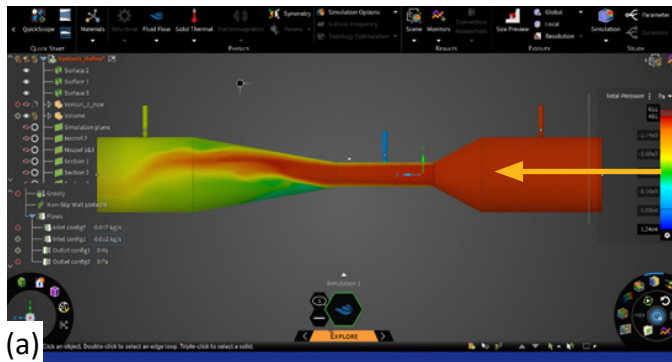


Figure 18: Venturi tube 1 Pressure Gradient Results. Flow direction indicated by yellow arrows
(a) Config. 1 and (b) Config. 2

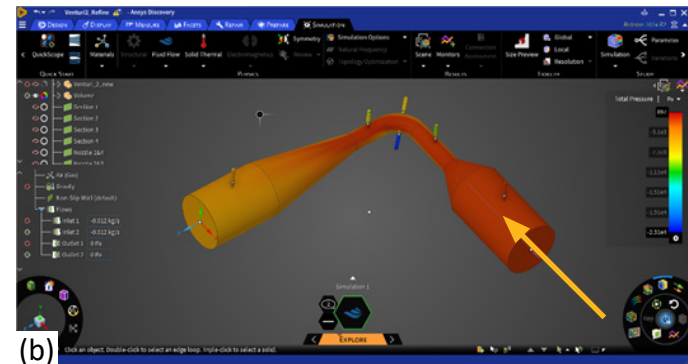
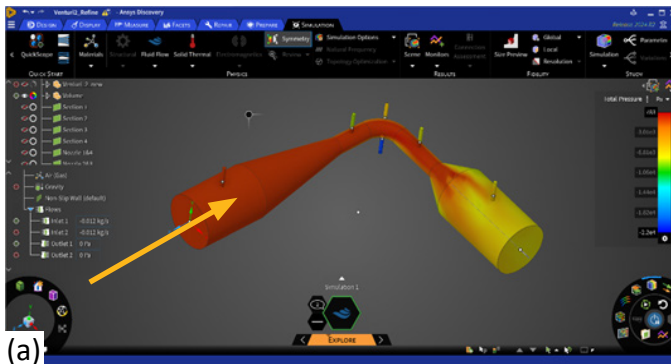


Figure 19: Venturi tube 2 Pressure Gradient Results. Flow direction indicated by yellow arrows
(a) Config. 1 and (b) Config. 2

7.3 Turbulence model sensitivity study

The Reynolds number describes whether a fluid flow tends to remain as laminar or transforms into turbulent flow by comparing the inertial force and viscous force in the fluid flow as shown by the formula below [3]:

$$Re = \frac{uL}{\nu} = \frac{\rho uL}{\mu} \quad \text{Eq. 4}$$

Where:

- Re is the Reynolds number
- u is the flow velocity in m/s
- L is the characteristic dimension in m
- ρ is the fluid density in kg/m³
- ν is the kinematic viscosity in m²/s
- μ is the dynamic fluid viscosity in Pa*s

Having low Reynolds numbers implies that the fluid tends to maintain its traveling direction and develop less turbulence, and having high Reynolds numbers implies that the fluid flow is more sensitive to interruptions and is easier to transform into turbulent flow.

There are a total of three different turbulence models available in the Ansys Discovery software for fluid behavior simulation, which are Laminar, Turbulent k-omega SST (SST), and Smagorinsky (LES).

Among all three models, Laminar treats fluid flow as orderly without any turbulence, which is expected to produce the most idealized, but also inaccurate fluid behavior simulation. SST, on the other hand, approximates flow separation and vortex structures to a moderate accuracy for steady state fluid flows. LES specializes in handling non steady state fluid flow which solves turbulence behavior by the furthest extent but usually requires extremely fine mesh density to generate reasonable results. However, the LES model is excluded from the comparison as it is only effective under the time dependent simulation, which is beyond the scope of this activity. To establish comparison between the performance of the two models, all tests and data discussed in the next section are carried out under the same boundary conditions, solid geometry, and constant fidelity.

7.3.1 Straight Venturi Tube Analysis

As shown in Figures 20a and b, the velocity and pressure profile under the Laminar model for Venturi tube 1 still exhibits some degree of fluctuation due to backflows.

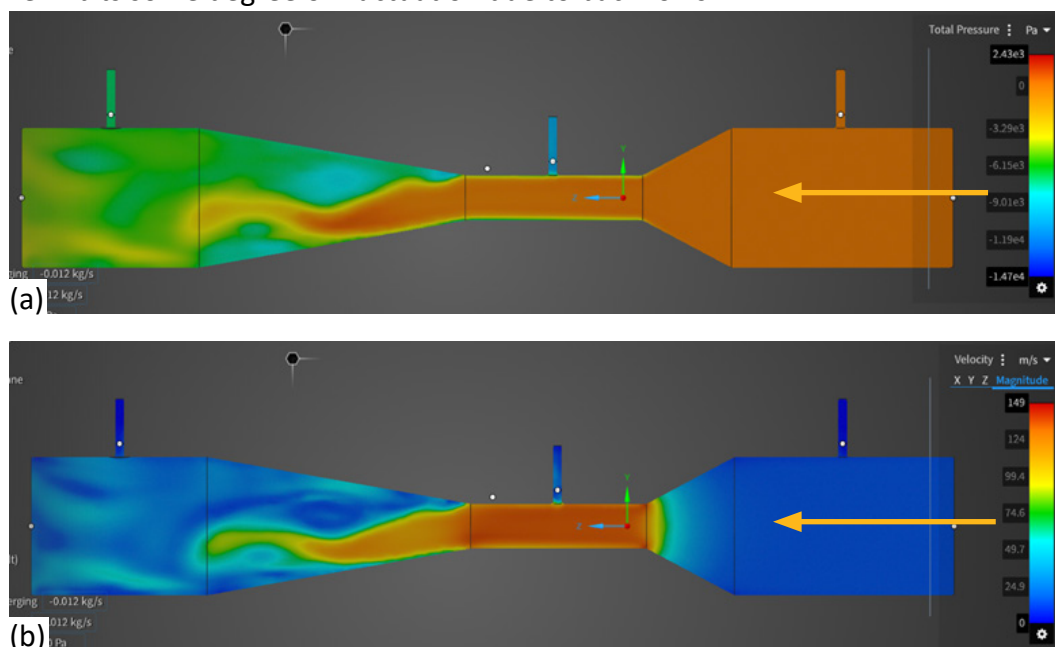


Figure 20: (a) Pressure Profile and (b) Velocity Profile for Venturi tube 1 under the Laminar Model

The velocity and pressure profile obtained using the SST model shows a relatively different fluid behavior after passing the throat section of the straight Venturi tube. As seen in Figures 21 a and b, the air stream bends downward rather than fluctuating before exiting from the other end of the Venturi tube. Comparing this behavior with the result from the Laminar model reveals that the SST model is more sensitive to the impact of disturbance on the fluid flow behavior.

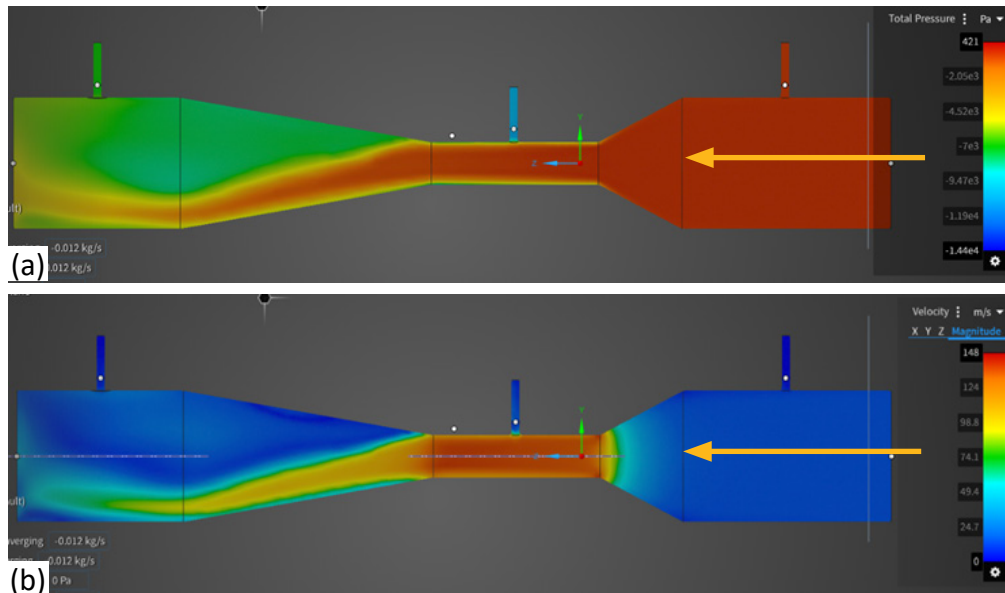


Figure 21: (a) Pressure Profile and (b) Velocity Profile for Venturi tube 1 under the SST Model.
 Flow direction indicated by yellow arrow

As seen from Table 7 and Table 8, the data taken at the same cross section is similar between the two models. The most significant difference in both the velocity and the pressure conditions takes place at the smooth converging end of the venturi tube, which may be a result of how the two models approach backflow disturbances differently. Overall, there is no noticeable improvement in accuracy between the laminar model and the SST model in the context of the standard Venturi tube. This is potentially because the solid geometry itself permits smooth fluid flow with minimal turbulence.

Table 7: Velocity Data Comparison of Standard Venturi Tube

Cross Section Location	Laminar (m/s)	SST (m/s)	% Absolute Difference
Smooth converging end	26.2	29.7	0.882%
Throat	121	121	1.000%
Acute converging end	13.3	13.4	0.993%

Table 8: Pressure Data Comparison of Standard Venturi Tube

Pressure Tap	Laminar (kPa)	SST (kPa)	Ratio
1	-0.106	-0.108	0.981
2	-10.3	-10.6	0.972
3	-6.1	-6.75	0.904

7.3.2 Twisted Venturi Tube Analysis

Taking one step further, the velocity profile and the pressure profile comparisons are presented in Figures 22 and 23 for Venturi tube 2. The laminar model showed considerable disturbances on the smooth converging end for both velocity and pressure profiles. In contrast, the SST model showed a much more gradual transition of velocity and pressure gradients. Based on Tables 8 and 9, the most

significant deviation of simulation results occurs at the smooth converging end of the Venturi tube with a considerable velocity ratio of 1.627 and a pressure ratio of 1.128. It is also observed that the two models have differences in pressure profile at the acute converging end, where the laminar model comes up with the pressure value that is 114% of the result solved by SST at the same location. It can be summarized from the results of both the standard venturi tube and the bent Venturi tube that the laminar model tends to over predict fluid behavior compared with SST.

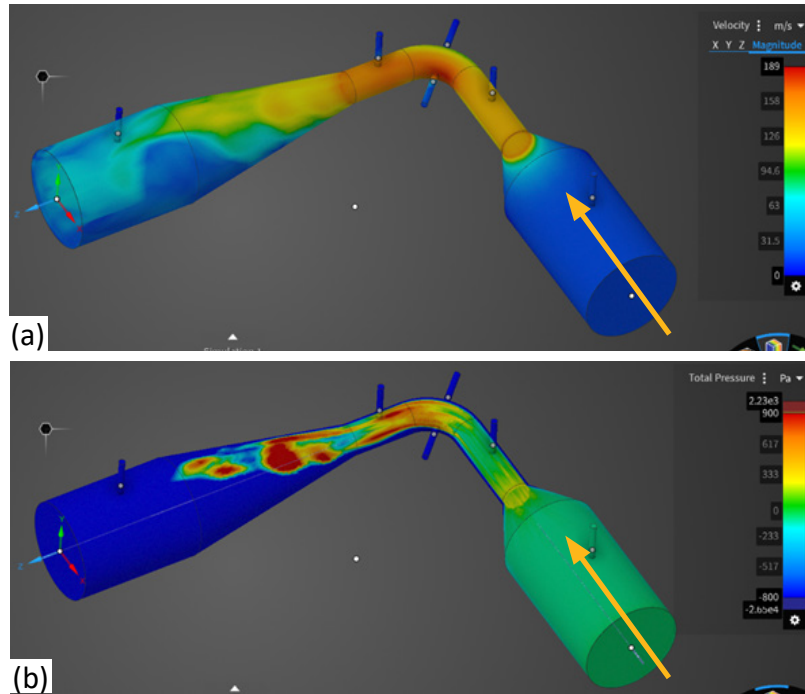


Figure 22: (a) Velocity Profile and (b) Pressure Profile for Venturi tube 2 under the Laminar Model
 Flow direction indicated by yellow arrow

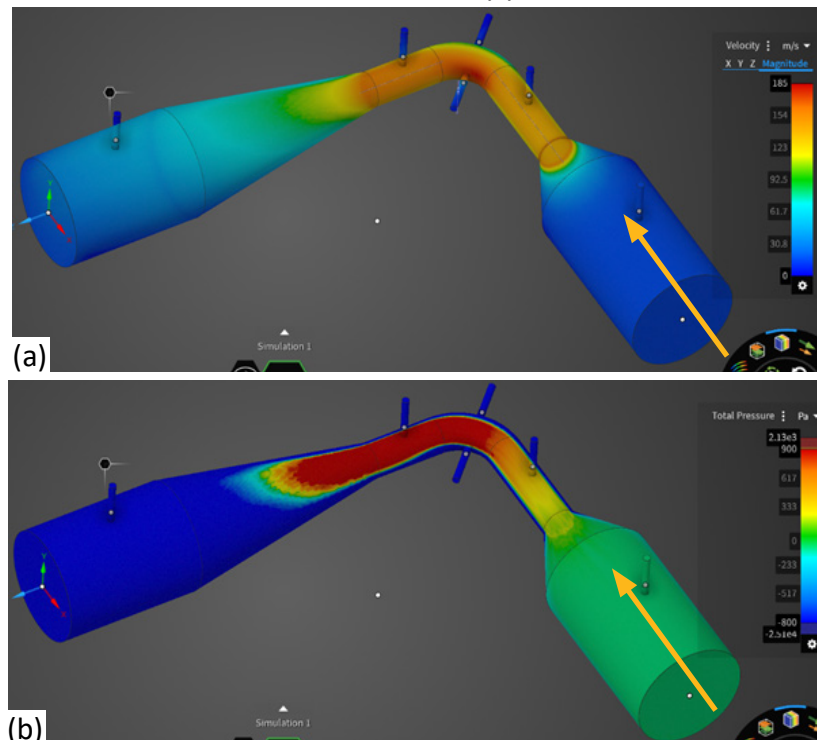


Figure 23: (a) Velocity Profile and (b) Pressure Profile for Venturi tube 2 under the SST Model
 Flow direction indicated by yellow arrow

Table 9: Velocity Data Comparison of Twisted Venturi Tube (Tube 2)

Cross Section Location	Laminar (m/s)	SST (m/s)	Ratio
Smooth converging end	30.1	18.5	1.627
Throat at the smooth converging end	129	127	1.016
Inner throat corner	142	140	1.014
Outer throat corner	72.8	71	1.025
Throat at the acute converging end	127	126	1.008
Acute converging end	13.7	13.5	1.015

Table 10: Pressure Data Comparison of Twisted Venturi Tube (Tube 2)

Pressure Tap	Laminar (kPa)	SST (kPa)	Ratio
1	-6.43	-5.7	1.128
2	-13.4	-12	1.117
Inner throat corner	-25.3	-24.4	1.037
Outer throat corner	-5.35	-5.94	0.901
3	-10.6	-10.5	1.010
4	-0.126	-0.11	1.145

8. Analysis

8.1 Air Velocity Profile

The values taken from the experiment with the venturi air velocity profile were graphed by reflecting the collected results across the y-axis to generate an approximate profile (see Figures 12 and 13). For all collections, the same vacuum was used which produced an outlet suction airspeed of approximately 12 m/s, found experimentally, as the airflow profile shows.

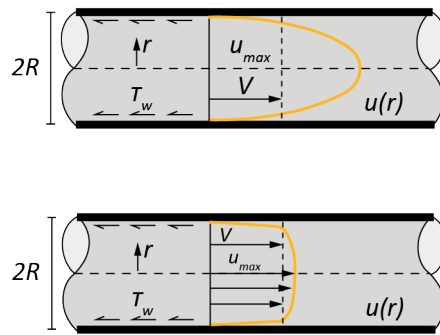


Figure 24: Velocity Distribution stabilized- laminar flow (top) and turbulent flow (bottom)

Experimental data showed that there exists a non-uniform velocity profile on the inlet of the venturi tube. The profile resembles that of a flattened parabola, while the flow profile of laminar flow is a sharper parabola. In multiple locations on the venturi tube, a cross section of the velocity gradient was taken, demonstrating this “parabolic” profile (Figures 25 and 26). There exists a peak velocity at the center of the tube, with reduction at the edges caused by the friction from the wall acting on the air. The laminar profile can be calculated via the following formula [2]:

$$v = v_{max} \left[1 - \left(\frac{r}{R} \right)^2 \right] \quad \text{Eq. 5}$$

Where:

- V is the laminar velocity profile
- R is the tube radius
- V_{max} is the max velocity (centerline velocity)
- r is radial distance from the pipe's center

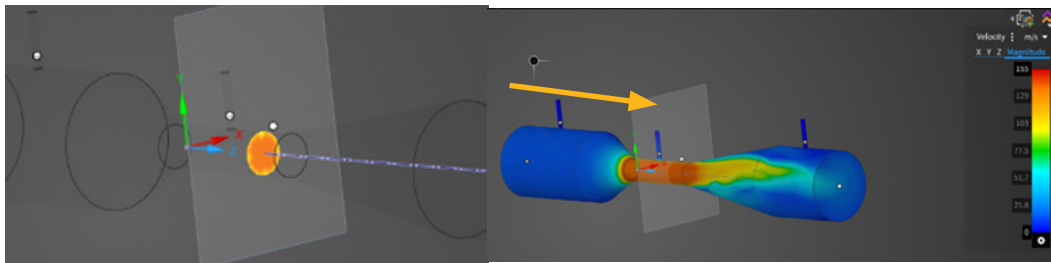


Figure 25: Converged Velocity Profile of Venturi 1. Flow direction indicated with yellow arrow



Figure 26: Outlet Velocity Profile of Venturi 1

Using the mouse to hover over the cross-section surface shows the exact velocity at the center versus the edge (shown on the scale as the mouse is moved). The velocity gradient is more easily visible at the throat, but still exists at the outlet upon closer inspection.

8.2 Sources of Error

8.2.1 Air leak

While collecting the experimental data for the Venturi, it was noted that there existed slight air leakage at each of the pressure taps as well as the connection point between the vacuum and the tube. This air leakage causes a decrease in the suction power of the system due to the decreased amount of airflow through the inlet. As a result, the overall velocity of the air flowing through the tube will decrease, affecting the pressure inside the tube. The relationship between velocity and pressure is inversely related, meaning that as the air velocity decreases, the pressure inside the venturi tube will increase. Following this reasoning, the experimental data should exhibit lower inlet velocities and higher pressures than the simulation since there exists no air leakage in the simulated experiment.

8.2.2 Meshing

The simulation results addressed in the case study used the mesh density of 85,319 elements and 28,830 nodes. However, in the simulation model, the values determined by the program are only as good as the model itself. This model requires a multitude of parameters to declare the proper materials, physics conditions, and boundary conditions, all of which will not be exactly the same as the simulation.

One parameter that will affect the results accuracy at a finer level is the model's meshing. The method that is used to divide the model into its elements and the size of the elements which are further used to calculate simulated results of the body, can greatly affect the results that are extrapolated from it. If the model has too low a mesh density, the elements will be very large which causes some of the data in those elements to be lost. Since each element is calculated to a single value, a large element could contain the peak value in the model along with low values surrounding it that reduce the overall element value. The true peak value of the model will not correspond with this meshing method, in the same way it will not correspond directly to other meshing methods with different sized elements.

8.2.3 Refine Mode

The simulation result under the “refine” mode is significantly different from that of the explore mode. The potential cause of the vast difference may be the highly customizable simulation options including utilization of LiveGX solver, meshing methods, fluid mesh quality, and automatic quality update according to local mesh density. The new configurations and features in refine mode may have also introduced more parameters into the final solution compared with solutions under the explore mode. On the other hand, this implies that the explore mode solutions may have limited depth in context specific problems as it provides limited simulation options and cannot be optimized further according to the specific simulation setup, which can lead to a faster but less accurate simulation result. Figures 27 and 28 show the different results acquired using both Explore and Refine modes.

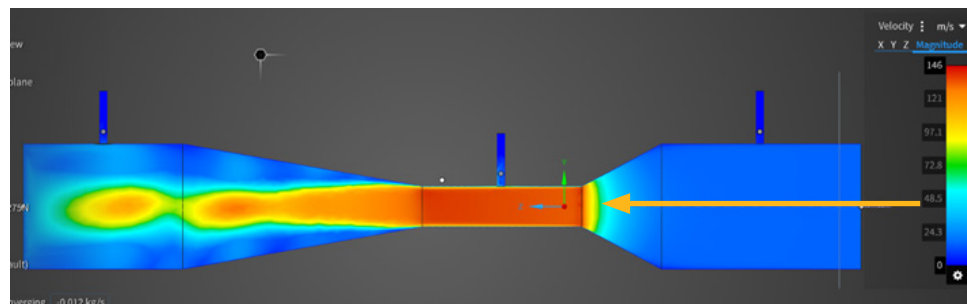


Figure 27: Max Fidelity in Refine Mode. Flow direction indicated with yellow arrow

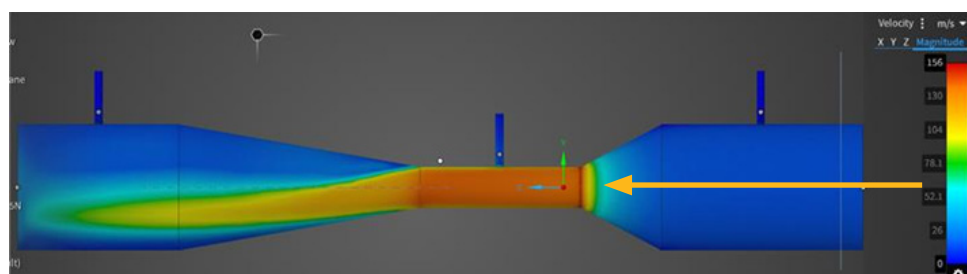


Figure 28: Max Fidelity in Explore Mode. Flow direction indicated with yellow arrow

8.2.4 3D Printing Shrinking/Surface Roughness

Sources of error are identified in the experimental apparatus manufacturing processes because filament 3D printing naturally has limited precision and accuracy compared to machining. Since the venturi tubes were 3D printed with filament, which would naturally induce layer lines on the surface of the model. The course surface can induce microscopic eddies that significantly interrupt the air velocity near the Venturi tube boundaries. This would result in disagreement with the simulation results in Ansys Discovery software, which assumed boundaries to be non-slip walls with no friction.

Additionally, PLA, which is the filament material used to print the Venturi tube models, usually experience shrinkage by around 0.5% after extrusion that can contribute to errors in experimental data. Specifically, the shrinkage in solid geometry would have allowed less unit air intake, and subsequently generate a exaggerated velocity measurement

8.2.5 Turbulence

Different turbulence models approach turbulence behavior differently. The model utilized for data collection and comparison with the experimental data in the case study is turbulent k-omega SST, which is often regarded as the most widely applied industrial grade model for turbulence approximation. According to K-Omega Turbulence Models, an article published by Simscale, the downside of such model is over prediction of turbulence magnitude at regions with rapid change in velocity [4]. For instance, the model tends to generate exaggerated turbulence behavior at points where fluid comes to a rapid stop or at locations where fluid rapidly speed up. Such limitation may influence the accuracy of fluid behavior at the three pressure taps, where fluid velocity dropped to near stagnation immediately after entering the pressure tap. This may have contributed to the significant error rate in pressure measurements.

9. Conclusions

This study analyzed the behavior of air flow through a Venturi tube using both experimental measurements and simulated data using Ansys Discovery software. The investigation focused on velocity and pressure variations along the tube, guided by Bernoulli's principle and the continuity equation.

Key findings indicate that as the throat diameter decreases, velocity increases and pressure decreases, confirming theoretical expectations. The tubes also experienced a parabolic velocity profile due to friction at the boundaries. This meant that velocity was higher at the center of the tube than at the edges.

Experimental results demonstrated the effects of turbulence, surface roughness and other sources of error, which contributed to variations in the measured values. Simulation data largely aligned with experimental results but showed greater deviation in Venturi 2, likely due to the model's asymmetry which could result in flow separation and backflow.

It was noted that configurations in which the steep side of the venturi tube was connected to the vacuum resulted in higher turbulence levels due to the more abrupt change in geometry. In contrast, when the smooth side was connected to the vacuum, the flow expanded more gradually, reducing the risk of flow separation and ensuring a smoother pressure recovery. A gradual expansion allowed the pressure to increase more evenly, keeping the boundary layer attached for a longer distance and

reducing turbulence.

10. References

- [1] International Organization for Standardization, “Measurement of fluid flow by means of pressure differential devices inserted in circular cross-section conduits running full — Part 4: Venturi tubes,” ISO Standard 5167-4:2022, 2022.
- [2] J. Stigler, “Analytical Velocity Profile in Tube for Laminar and Turbulent Flow,” Engineering MECHANICS, vol. 21, no. 6, pp. 371–379, 2014, Accessed: Mar. 17, 2025. [Online]. Available: http://www.engineeringmechanics.cz/pdf/21_6_371.pdf
- [3] F. Menter, “Laminar vs. Turbulent Flow: Difference, Examples, and Why It Matters,” Ansys.com, Jan. 06, 2025. <https://www.ansys.com/blog/laminar-vs-turbulent-flow> (accessed Mar. 17, 2025).
- [4] Simscale, “K-omega SST I Global Settings I SimScale Documentation,” SimScale, May 25, 2021. <https://www.simscale.com/docs/simulation-setup/global-settings/k-omega-sst/> (accessed Mar. 17, 2025).

Textbook used for reference information: Measurement of Flow Rate, Velocity Profile and Friction Factor in Pipe Flows

© 2025 ANSYS, Inc. All rights reserved.

Use and Reproduction

The content used in this resource may only be used or reproduced for teaching purposes; and any commercial use is strictly prohibited.

Document Information

This case study is part of a set of teaching resources to help introduce students to structures, fluids, or heat transfer (physics areas supported by Ansys Discovery).

Ansys Education Resources

To access more undergraduate education resources, including lecture presentations with notes, exercises with worked solutions, microprojects, real life examples and more, visit www.ansys.com/education-resources.

Feedback

Here at Ansys, we rely on your feedback to ensure the educational content we create is up-to-date and fits your teaching needs.

Please click the link here out a short survey (~7 minutes) to help us continue to support academics around the world utilizing Ansys tools in the classroom.

ANSYS, Inc.
Southpointe
2600 Ansys Drive
Canonsburg, PA 15317
U.S.A.
724.746.3304
ansysinfo@ansys.com

If you've ever seen a rocket launch, flown on an airplane, driven a car, used a computer, touched a mobile device, crossed a bridge or put on wearable technology, chances are you've used a product where Ansys software played a critical role in its creation. Ansys is the global leader in engineering simulation. We help the world's most innovative companies deliver radically better products to their customers. By offering the best and broadest portfolio of engineering simulation software, we help them solve the most complex design challenges and engineer products limited only by imagination.

visit www.ansys.com for more information

Any and all ANSYS, Inc. brand, product, service and feature names, logos and slogans are registered trademarks or trademarks of ANSYS, Inc. or its subsidiaries in the United States or other countries. All other brand, product, service and feature names or trademarks are the property of their respective owners.

© 2025 ANSYS, Inc. All Rights Reserved.